Eur. J. Mech. B - Fluids 19 (2000) 391–402

S0997-7546(00)00117-5/FLA

Isolated solitary vortex solutions for the Ekman Couette layer

Norbert P. Hoffmann, Friedrich H. Busse *

Institute of Physics, University of Bayreuth, 95440 Bayreuth, Germany

(Received 21 June 1999; revised 8 February 2000; accepted 21 February 2000)

Abstract – Isolated solutions have been found describing solitary vortex motions in a fluid layer between two parallel plates moving relative to each other in a system that rotates about an axis normal to the plates. The solutions are called isolated since they do not seem to be connected by bifurcations to any other known solutions of the problem. The solitary vortex solutions are unstable with respect to three-dimensional disturbances, but attempts to find three-dimensional steady states have not yet been successful. © 2000 Éditions scientifiques et médicales Elsevier SAS

solitary vortex solution / Ekman Couette layer

1. Introduction

The Ekman–Couette layer is obtained when two rigid parallel plates move relative to each other with the constant velocity $\boldsymbol{U}_d$ in a system rotating with the angular velocity vector $\boldsymbol{\Omega}_d$ normal to the plates. This configuration is realized experimentally in a local sense when two parallel disks are rotating with different angular velocities about their common axis. Even if the angular velocity of one of the disks vanishes the theory of the Ekman–Couette layer still appears to be applicable as the comparison of computational results with the experimental measurements suggests (Schouveiler et al. [1]; Hoffmann et al. [2]). There are three different types of instability.

For low values of the dimensionless rotation parameter Ω the instability in the form of Ekman–Couette rolls occurs first. These rolls are point symmetric with respect to their axis on the midplane of the layer and are stationary with respect to the reference system of vanishing averaged mass flux. The other two instabilities are the Ekman layer instabilities of types I and II which occur in the Ekman boundary layers attached to the rigid plates and are asymmetric with respect to the midplane of the layer. There are thus two modes in the form of waves traveling along the respective boundaries for each of the instabilities of type I and type II. The secondary states of motion that evolve from these instabilities have been studied in a recent paper (Hoffmann et al. [2]) where also bifurcations to tertiary states of fluid flow have been analyzed. Serendipitously still another state of fluid flow has been discovered in the course of this work which will be described in the following. This new solution of the basic equations of motion does not seem to bifurcate from any other known solution. It exists at low Reynolds numbers where the basic state is still stable with respect to infinitesimal disturbances. The new solution is isolated also in other respects in that it describes a solitary type vortex. Disturbances in the form of single solitary waves, also called ‘rollers’, have been observed in several experiments (San’kov and Smirnov [3]; Schouveiler et al. [1]). The fact that the parameter regime of the observations corresponds roughly to the regime where the isolated rolls have been found theoretically has motivated us to carry out the detailed analysis reported in this paper. It is hoped that future experiments will shed more light on this unusual phenomenon.

* Correspondence and reprints; e-mail: busse@uni-bayreuth.de

2. Mathematical description of the problem

We consider a layer of an incompressible fluid between two parallel plates moving with the constant velocity $\boldsymbol{U}_d$ relative to each other in a system which rotates with angular velocity $\boldsymbol{\Omega}_d$ about an axis normal to the plates as shown in *figure 1*. Using the distance h between the plates as length scale and h^2/ν as time scale where ν is the kinematic viscosity of the fluid we can write the Navier–Stokes equations in dimensionless form

$$\frac{\partial}{\partial t}\boldsymbol{v} + \boldsymbol{v}\cdot\nabla\boldsymbol{v} + 2\Omega\boldsymbol{k}\times\boldsymbol{v} = -\nabla\pi + \nabla^2\boldsymbol{v}, \tag{1a}$$

$$\nabla\cdot\boldsymbol{v} = 0, \tag{1b}$$

where $\boldsymbol{k}$ is the unit vector normal to the plates and π is the dynamic pressure. Using a Cartesian system of coordinates with the z-coordinate in the direction of $\boldsymbol{k}$ we write the boundary condition in the form

$$\boldsymbol{v} = \mp\frac{1}{2}Re\,\boldsymbol{i} \quad \text{at } z = \pm\frac{1}{2}, \tag{2}$$

where $\boldsymbol{i}$ is the unit vector in the x-direction. The dimensionless parameters Re and Ω are defined by

$$Re \equiv U_d h/\nu, \qquad \Omega \equiv \Omega_d h^2/\nu. \tag{3}$$

The basic steady solution of equations (1) together with conditions (2) is given by

$$\boldsymbol{v} = \boldsymbol{U}_0 = \big(U_{0x}(z), U_{0y}(z), 0\big) \tag{4}$$

with

$$U_{0x} = -A\sin\sqrt{\Omega}z\cosh\sqrt{\Omega}z + B\cos\sqrt{\Omega}z\sinh\sqrt{\Omega}z,$$
$$U_{0y} = A\cos\sqrt{\Omega}z\sinh\sqrt{\Omega}z + B\sin\sqrt{\Omega}z\cosh\sqrt{\Omega}z,$$

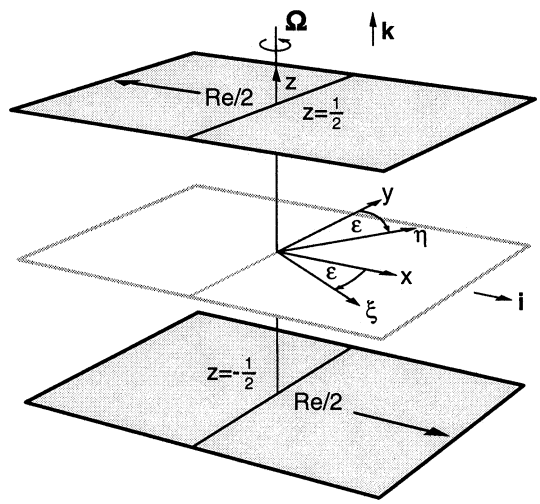

Figure 1. Geometrical configuration of the Ekman–Couette layer.

$$A\left\{\sin\frac{1}{2}\sqrt{\Omega}\cosh\frac{1}{2}\sqrt{\Omega}\right\}^{-1} = -B\left\{\cos\frac{1}{2}\sqrt{\Omega}\sinh\frac{1}{2}\sqrt{\Omega}\right\}^{-1}$$
$$= \frac{Re}{2}\left\{\sin^2\frac{1}{2}\sqrt{\Omega}\cosh^2\frac{1}{2}\sqrt{\Omega} + \cos^2\frac{1}{2}\sqrt{\Omega}\sinh^2\frac{1}{2}\sqrt{\Omega}\right\}^{-1}.$$

This solution clearly exhibits the Ekman layer structure near the boundaries $z = \pm\frac{1}{2}$ as Ω increases to large values. For vanishing Ω solution (4) reduces to the plane Couette flow $\boldsymbol{U}_0 = -Re\, z\boldsymbol{i}$.

In order to describe other solutions of equations (1) we use the general representation

$$\boldsymbol{v} = \boldsymbol{U} + \nabla\times(\nabla\phi\times\boldsymbol{k}) + \nabla\psi\times\boldsymbol{k} \equiv \boldsymbol{U} + \boldsymbol{\delta}\phi + \boldsymbol{\varepsilon}\psi \equiv \boldsymbol{U} + \boldsymbol{u} \tag{5}$$

for the solenoidal vector field $\boldsymbol{v}$ where the functions ϕ and ψ can be chosen without loss of generality such that their x, y-average – indicated by a bar – vanishes,

$$\bar{\phi} = \bar{\psi} = 0, \qquad \bar{\boldsymbol{v}} = \boldsymbol{U} \equiv \boldsymbol{U}_0 + \hat{\boldsymbol{U}}. \tag{6}$$

Using the z-components of the (curl)^2 and of the curl of equation (1a) we obtain two equations for ϕ and ψ,

$$\nabla^4\Delta_2\phi - 2\Omega\frac{\partial}{\partial z}\Delta_2\psi = \boldsymbol{k}\cdot\nabla\times\big(\nabla\times(\boldsymbol{u}\cdot\nabla\boldsymbol{u})\big) + \left(\frac{\partial}{\partial t} + \boldsymbol{U}\cdot\nabla\right)\nabla^2\Delta_2\phi - \frac{\partial^2}{\partial z^2}\boldsymbol{U}\cdot\nabla\Delta_2\phi, \tag{7a}$$

$$\nabla^2\Delta_2\psi + 2\Omega\frac{\partial}{\partial z}\Delta_2\phi = -\boldsymbol{k}\cdot\nabla\times(\boldsymbol{u}\cdot\nabla\boldsymbol{u}) + \left(\frac{\partial}{\partial t} + \boldsymbol{U}\cdot\nabla\right)\Delta_2\psi - \frac{\partial}{\partial z}\boldsymbol{U}\cdot\boldsymbol{\varepsilon}\Delta_2\phi, \tag{7b}$$

where the two-dimensional Laplacian, $\Delta_2 = \partial^2/\partial x^2 + \partial^2/\partial y^2$, has been introduced. The equation for the mean flow is given by

$$\left(\frac{\partial^2}{\partial z^2} - \frac{\partial}{\partial t}\right)\hat{\boldsymbol{U}} + 2\Omega\boldsymbol{k}\times\hat{\boldsymbol{U}} = -\frac{\partial}{\partial z}\overline{\left(\Delta_2\phi\left(\frac{\partial}{\partial z}\nabla_2\phi + \boldsymbol{\varepsilon}\psi\right)\right)}, \tag{7c}$$

where ∇_2 stands for the two-dimensional nabla operator, $(\partial/\partial x, \partial/\partial y, 0)$. The no-slip boundary conditions at the plates require

$$\phi = \frac{\partial}{\partial z}\phi = \psi = 0, \qquad \hat{\boldsymbol{U}} = 0 \quad \text{at } z = \pm\frac{1}{2} \tag{8}$$

for the numerical solution of equations (7) we use Galerkin representations for the dependent variables in terms of complete systems of functions which satisfy the boundary conditions (7),

$$\phi = \sum_{m,n} a_{mn}\exp\{ima\eta\}g_n(z), \tag{9a}$$

$$\psi = \sum_{m,n} b_{mn}\exp\{ima\eta\}\sin n\pi\left(z + \frac{1}{2}\right), \tag{9b}$$

$$\boldsymbol{U} = \sum_{n} \boldsymbol{d}_n\sin n\pi\left(z + \frac{1}{2}\right), \tag{9c}$$

where the coordinates ξ, η are related to x, y through the transformation

$$\begin{pmatrix}\xi\\ \eta\end{pmatrix} = \begin{pmatrix}\cos\varepsilon & -\sin\varepsilon\\ \sin\varepsilon & \cos\varepsilon\end{pmatrix}\begin{pmatrix}x\\ y\end{pmatrix} \tag{10}$$

and where the Chandrasekhar [4] functions $g_n(z)$ have been introduced. Solutions of the form (9) describe general two-dimensional states of flow which are independent of the direction of the ξ-axis which assumes the angle ε with respect to the x-axis. After the representations (9) have been introduced in equations (7) and the latter have been projected onto the expansion functions, a system of nonlinear equations for the unknown coefficients a_{mn}, b_{mn} and $\boldsymbol{d}_n = (d_{nx}, d_{ny}, 0)$ is obtained. We first shall look for steady solutions in which case the system of algebraic equations can be solved through a Newton–Raphson iteration method. In the case of time dependent solutions the unknown coefficients are functions of time and a system of ordinary differential equations in time are obtained which can be solved through forward integrations with a Runge–Kutta method.

In the case of a steady solution it is easy to determine its stability with respect to infinitesimal perturbations through the superposition of general disturbances of the form

$$\tilde{\phi} = \exp\{ib\xi + id\eta + \sigma t\} \sum_{mn} \tilde{a}_{mn} \exp\{ima\eta\} g_n(z), \tag{11a}$$

$$\tilde{\psi} = \exp\{ib\xi + id\eta + \sigma t\} \sum_{mn} \tilde{b}_{mn} \exp\{ima\eta\} \sin n\pi \left(z + \frac{1}{2}\right). \tag{11b}$$

Introduction of these representations into equations (7) which are linearized about the steady solution of the form (9) yields an eigenvalue problem for the growth rate σ. Whenever there exists an eigenvalue σ with a positive real part as a function of the Floquet wavenumbers d and b, the steady solution is unstable; otherwise it will be regarded as stable.

In the numerical implementation of the Galerkin representations (9) and (10) the infinite sums must be truncated. We shall neglect all coefficients and corresponding equations satisfying the truncation condition

$$n + m > N_t, \tag{12}$$

where N_t is a natural number which has been set equal to 10 or higher in the computations. Whenever significant changes with respect to the results obtained for $N_t + 2$ have been noticed, higher values of N_t up to $N_t = 16$ have been used.

3. Steady solitary vortex solutions

Steady spatially periodic roll solutions of the form (9) bifurcating from the basic static state (4) have been studied in the previous paper (Hoffmann et al. [2]). Here we present isolated branches of steady solutions describing solitary vortices. The structure of these new solutions is exhibited in *figure 2*. While the same representation is used as for the previously studied Ekman–Couette rolls, the wavenumber a obviously does not characterize the diameter of the roll like vortex which remains rather independent of the periodicity length as long as the latter is sufficiently large. Numerical limitations do not allow us to decrease a much below the value of 0.6 corresponding to the largest aspect ratio displayed in *figure 2*. However,there can be little doubt that the solitary roll solution exists also in the limit $a \to 0$ as we shall discuss below in more detail in connection (section 3). For this reason we call this type of solution the solitary vortex, even though it is not truly solitary for finite values of a.

A remarkable property of this type of solution is that it exists also in a region of the $Re - \Omega$ parameter space where the basic solution (4) is stable with respect to infinitesimal disturbances. This property is demonstrated in *figure 3* where the lowest values of Re for which the solitary vortex solution can be obtained is shown as a function of Ω. There is clearly a substantial interval, $12 \leqslant \Omega \leqslant 80$, in which the solitary vortex solution exists at values of the Reynolds number Re below those at which other secondary states of motions can exist. Since

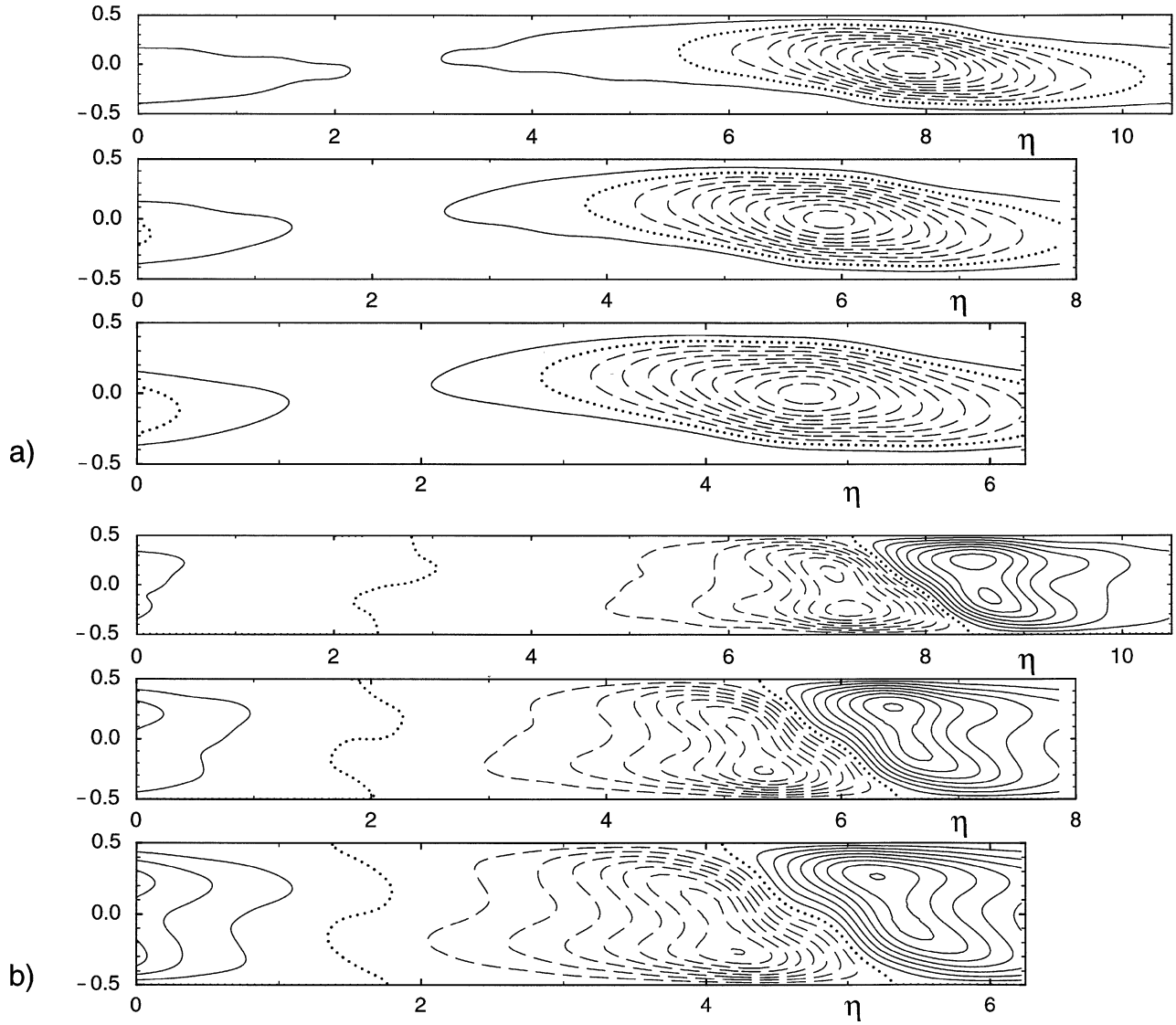

Figure 2. (a) Streamlines of the solitary vortex solution in the η-z-plane for $R = 550, \Omega = 25, \varepsilon = 26.4°$. The plots correspond to $a = 0.6, 0.8$ and 1.0 (from top to bottom). Solid (dashed) lines indicate positive (negative) values of $\partial\varphi/\partial\eta$. The values of $\partial\varphi/\partial\eta$ change by 2.22 from one line to the next. The dotted line indicates $\frac{\partial\varphi}{\partial\eta} = 0$. (b) Lines of constant ξ-component of the velocity for the same parameters as above. The value of the ξ-velocity changes by 18.75 from one line to the next.

the latter correspond to supercritical bifurcations, the instability curves also give the lowest values of Re for their existence. Also shown in *figure 3* is the orientation angle ε of the vortex axis with respect to the applied shear. This angle is somewhat larger than for the other solutions, but does not differ dramatically. There is a finite range of angles ε which does increase as the parameter a decreases as shown in *figure 4(a)*. The range of angles ε for which solutions exist also broadens as the Reynolds number increases for a given value of a as indicated in *figure 4(b)*. These properties suggest that the lowest Reynolds numbers for the existence of the solitary vortex solution is approached in the limit $a \to 0$ which can not be reached with the presently used

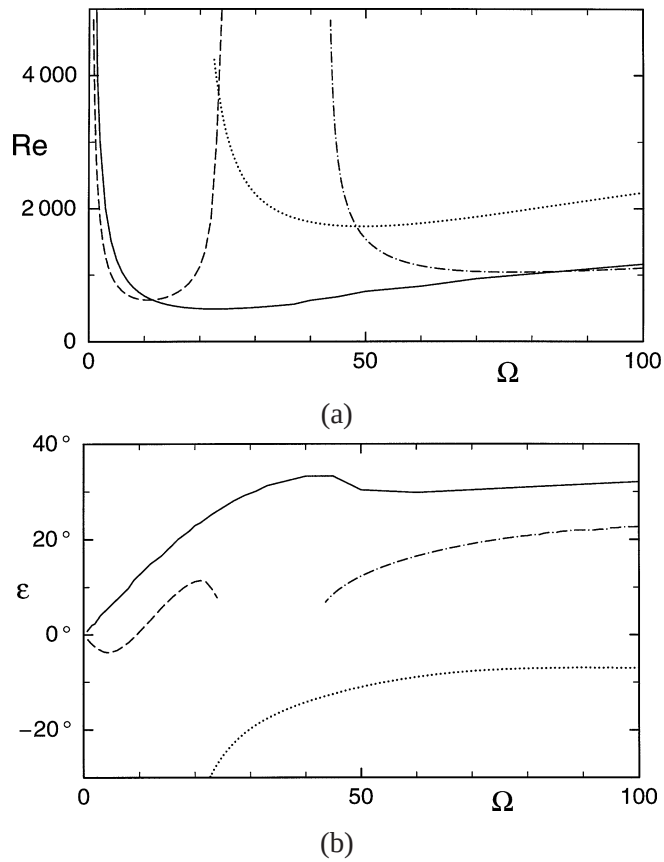

Figure 3. (a) Minimal Reynolds number Re for the existence of solitary vortex solutions (solid line) in comparison with the onset of Ekman–Couette rolls (dashed line) and type I (dotted line) and type II (dash-dotted line) Ekman instabilities.
(b) The angle ε corresponding to the lines shown in plot (a).

numerical scheme. The line drawn in *figure 3* corresponds to results obtained for $a \approx 0.8$. But it is not expected that it will move significantly if a is decreased further.

The structure of the solitary vortex solution does not change much as ε is varied as can be seen from the plots of *figure 5*. Only the amplitude changes and reaches its largest value in middle of the range of possible ε-values. Besides the solutions of *figure 5* corresponding to the 'upper' branch there is also a 'lower' branch corresponding to a lower amplitude of the solitary vortex such that there is a closed surface in the form of a tongue in the Re-ε-space for given values of the parameters a and Ω. In *figure 6* a cut through this surface is shown as an example. Here the shear ratios S_ξ and S_η have been introduced as measures of the amplitude. They are defined by

$$S_\xi = S_x \cos\varepsilon - S_y \sin\varepsilon, \qquad S_\eta = S_x \sin\varepsilon + S_y \cos\varepsilon, \tag{13a}$$

where

$$S_x = 1 + \sum_n n\pi d_{nx} \Big/ \left.\frac{\partial U_{0x}}{\partial z}\right|_{z=\frac{1}{2}}, \qquad S_y = 1 + \sum_n n\pi d_{ny} \Big/ \left.\frac{\partial U_{0y}}{\partial z}\right|_{z=\frac{1}{2}} \tag{13b}$$

has been used. These shear ratios describe the fractional increase or decrease of the shear at the boundary in the respective direction due to the presence of the solitary vortex solution. The quantities $S_\xi - 1$ and $S_\eta - 1$ vary,

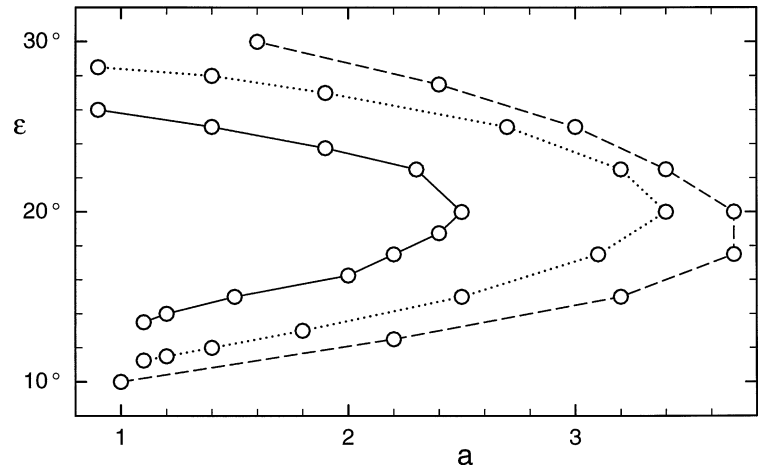

(a)

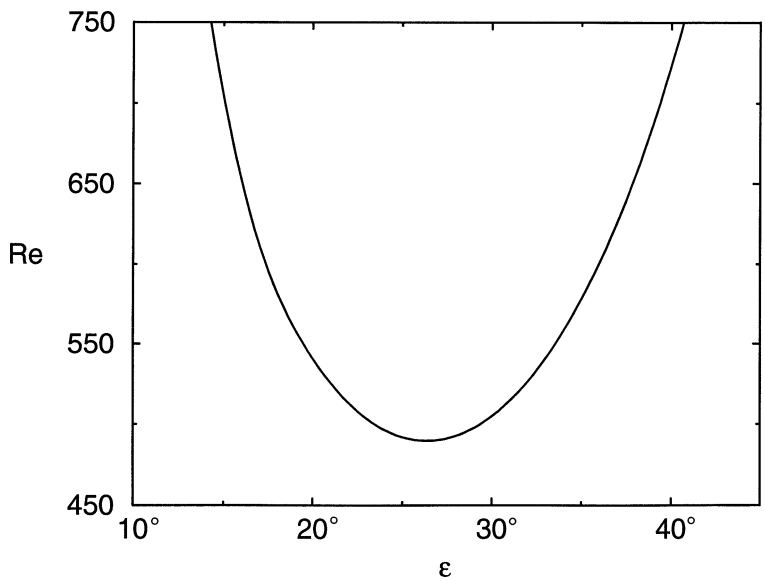

(b)

Figure 4. (a) Range of angles ε for which solitary vortex solutions exist as function of a in the case $\Omega = 17$ for $Re = 600$ (solid line), $Re = 700$ (dotted line) and for $Re = 800$ (dashed line). (b) Range of angles ε for which solitary vortex solutions exist as a function of Re in the case $a = 0.8$, $\Omega = 25$.

of course, approximately linearly with a as can be seen in the plots of *figure 7* because there is always only one solitary vortex in the interval $0 \leqslant \eta \leqslant 2\pi/a$ over which the shear has been averaged. Because the numerical description of the solitary vortex solution becomes especially demanding in the case of low values of a different degrees of numerical approximation have been compared in *figure 7*. The truncation parameter $N_t = 16$ appears to be sufficient for values of a down to $a = 0.8$. At higher values of a of the order 2, the solitary vortex causes a substantial change in the shear exerted at the boundary especially if it is compared with the shear exerted by the Ekman–Couette rolls with comparable wavelength. Such a comparison is shown in *figure 8* where S_ξ and S_η have been plotted in dependence on the Reynolds number.

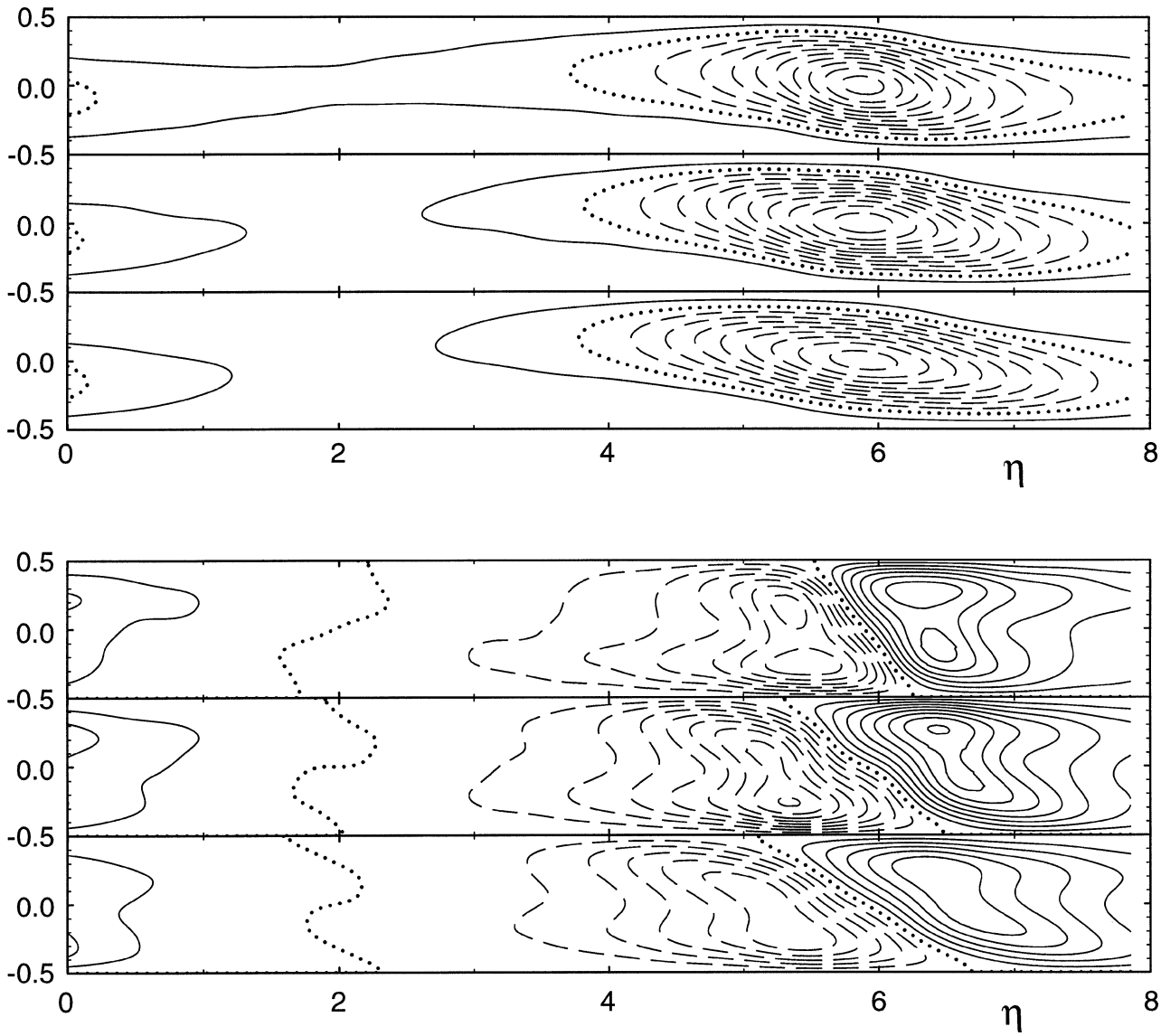

Figure 5. Streamlines of the solitary vortex solution in the η-z-plane for $\varepsilon = 19.5°, 26.4°, 33.2°$ (upper three plots from top) and corresponding plots of the lines of constant ξ-component of the velocity (lower three plots) in the case $Re = 550$, $\Omega = 25$, $a = 0.8$. The values of the streamlines change by 2.22 from one line to the next and the values of the ξ-velocity change by 21.4 from one line to the next except in the case $\varepsilon = 26.4°$ where the change is 18.75.

For increasing Ω and Re the solitary vortex becomes more localized and instead of a single maximum of its strength on the midplane of the layer it develops two maxima near the boundaries as shown in *figure 9*. This property reflects the increasing shears in the Ekman layers which develop with increasing Ω. While for low Ω the vortex is rather extended in the η-direction as can be seen in the two uppermost plots of the figure, the diameter of the vortex tends to become less than the height of the layer for large Ω and Re.

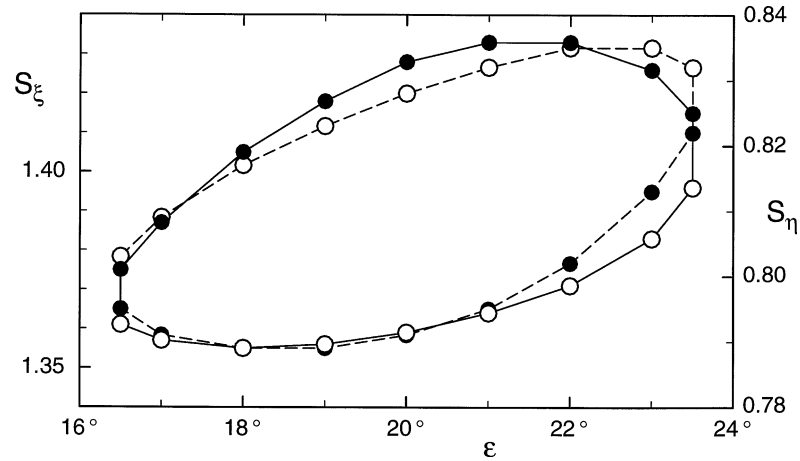

Figure 6. The shear ratios S_ξ (left ordinate, symbols connected by solid lines) and S_η (right ordinate, symbols connected by dashed lines) as a function of the angle ε in the case $Re = 600, \Omega = 17, a = 2.0$. Filled (open) circles correspond to solutions of the upper (lower) branch.

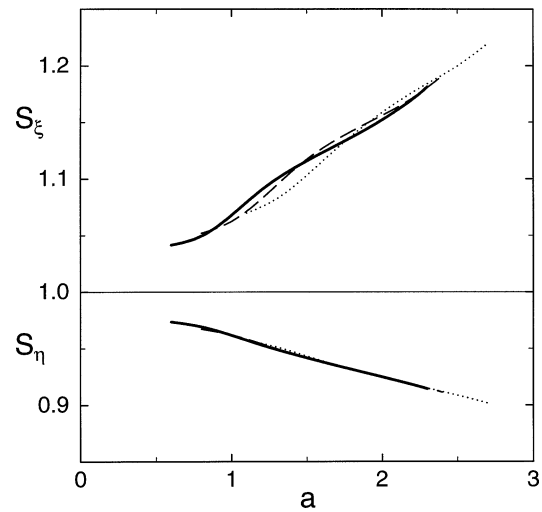

Figure 7. The shear ratios S_ξ and S_η as a function of a in the case $Re = 1000, \Omega = 70, \varepsilon = 30.4°$. The dotted, dashed and solid curves have been obtained for the truncation parameters $N_t = 12, 14$ and 16, respectively.

4. Instabilities of the solitary vortex solution

As discussed in section 2 the growth rates σ of arbitrary infinitesimal three-dimensional disturbances can be computed as eigenvalues of the stability problem in dependence on the wavenumbers b and d for a given steady solitary vortex solution. It is found that the Floquet wavenumber d has relatively little influence on the eigenvalues and that the maximum values of the real parts σ_r correspond to $d = 0$ in all cases. This property is a consequence of the solitary nature of the vortex which is not sensitive to changes in the wavenumber a.

The dependence on b is more interesting and typical examples are shown in *figure 10*. The highest growth rates σ_r are characterized by vanishing imaginary parts of σ and exhibit two maxima at $b = 0$ and at a finite value of b which increases with Re. This situation is typically found for the upper branch of the solution characterized by a higher value of S_ξ than the lower branch. The maximum of σ_r at the finite value of b exceeds

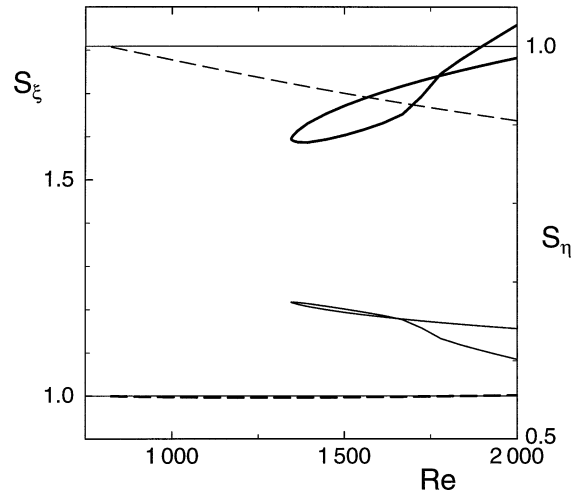

Figure 8. The shear ratios S_ξ (thick lines, left ordinate) and S_η (thin lines, right ordinate) as function of Re for the Ekman rolls (dashed lines bifurcating from the line $S_\xi = S_\eta = 1$) and for the solitary vortex solution, both with $a = 2.25$, in the case $\Omega = 17$, $\varepsilon = 8°$.

that at $b = 0$ for lower values of Re and Ω while the opposite property is found for larger values of Re and Ω. For the lower branch, on the other hand, the growth rate σ_r appears to reach its highest value always at a finite value of b which is smaller than 1, but increases with decreasing Re. As Re reaches the minimum value of about 500 the growth rate spectra of upper and lower branch approach each other as must be expected for reasons of continuity. While the upper solution exhibits a higher amplitude than the lower solution it still appears to be always unstable even though the growth rates are usually much smaller than for the lower solution.

Numerous attempts have been made to follow the evolution of growing disturbances through forward integrations in time for values of b where σ_r reaches a maximum as well as those values where σ_r is only slightly positive. In all cases, however, the integrations have led asymptotically to the primary state (4) unless the parameters Re and Ω were chosen such that other secondary solutions as, for instance, the Ekman–Couette rolls were available as attractors.

5. Concluding remarks

Solitary vortices of the kind considered in this paper do not occur as rarely as it may appear. In the case of a layer of a low Prandtl number fluid heated from below nearly circular rolls with essentially an arbitrary distance between them can be found (Clever and Busse [5]). These rolls represent a manifestation of inertial convection which is characterized by a substantially higher heat transport than the ordinary spatially periodic convection rolls that set in at the critical value of the Rayleigh number. Unfortunately, the solitary convection rolls are unstable just as the solitary vortices in the Ekman–Couette layer.

Solitary transverse vortices have also been found as finite amplitude solution in the problem of plane Couette flow (Cherhabili and Ehrenstein [6]). This finding has suggested to us that there may be a connection between the solitary solutions of both problems since the plane Couette case corresponds to the limit $\Omega \to 0$ of the problem described by equations (7). A detailed numerical study of this limit has shown, however, that such a connection does not seem to exist. The Reynolds number for the existence of the solitary vortex solution tends to infinity as $\Omega = 0$ is approached and the angle ε does not indicate a tendency to grow towards 90°. Also the form of the vortex differs from that found by Cherhabili and Ehrenstein [7].

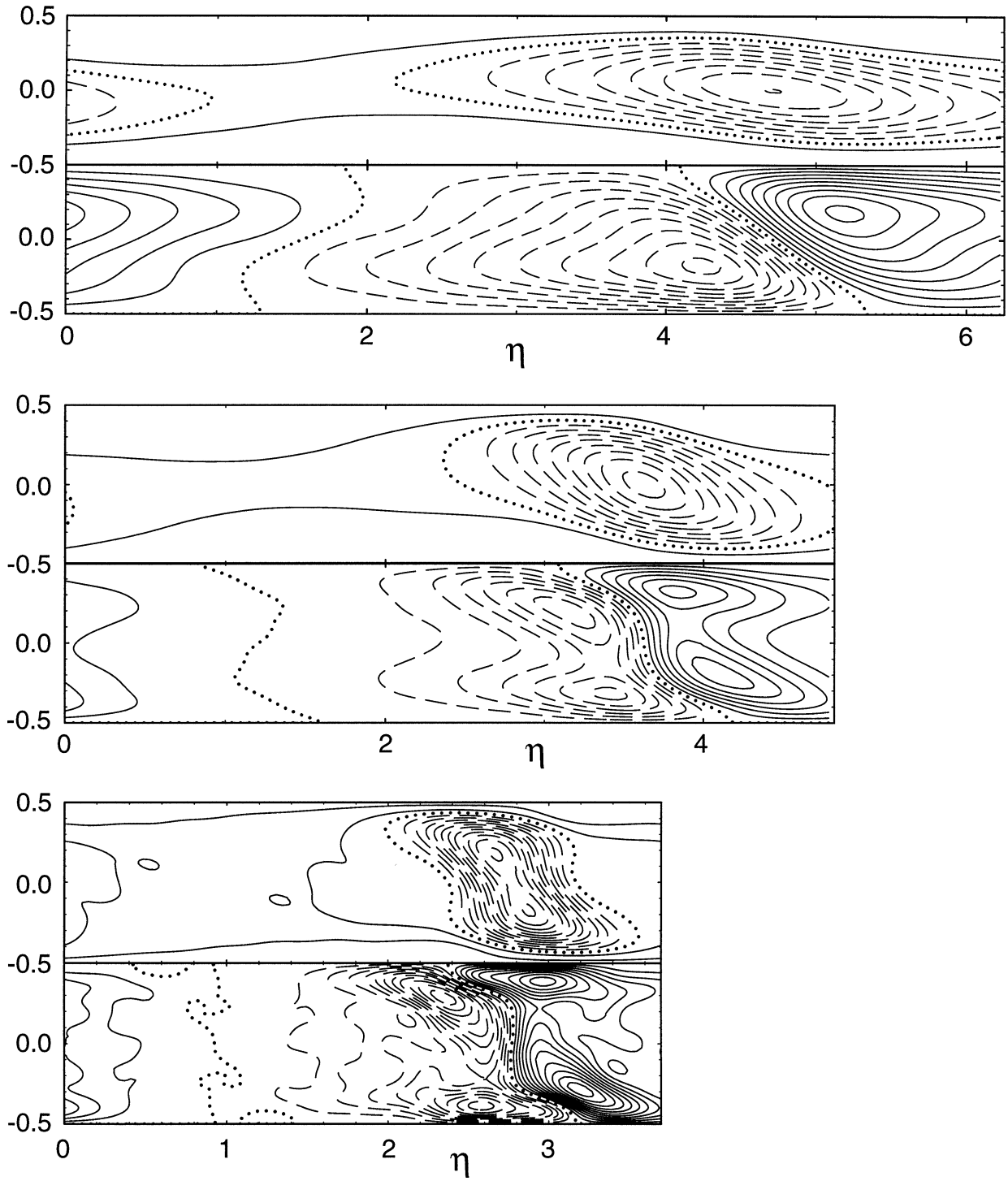

Figure 9. Streamlines together with corresponding plots of constant ξ-velocity of the solitary vortex solution in the η-z-plane and in the cases $\Omega = 10$, $Re = 685$, $\varepsilon = 12.6°$ (upper two plots); $\Omega = 40$, $Re = 700$, $\varepsilon = 32.7°$ (middle two plots) and $\Omega = 100$, $Re = 1170$, $\varepsilon = 33.2°$ (lower two plots). The values of the streamlines change by 2.18 from one line to the next and the values of the ξ-velocity change by 20.8 except in the case $\Omega = 10$ where the change is 27.8.

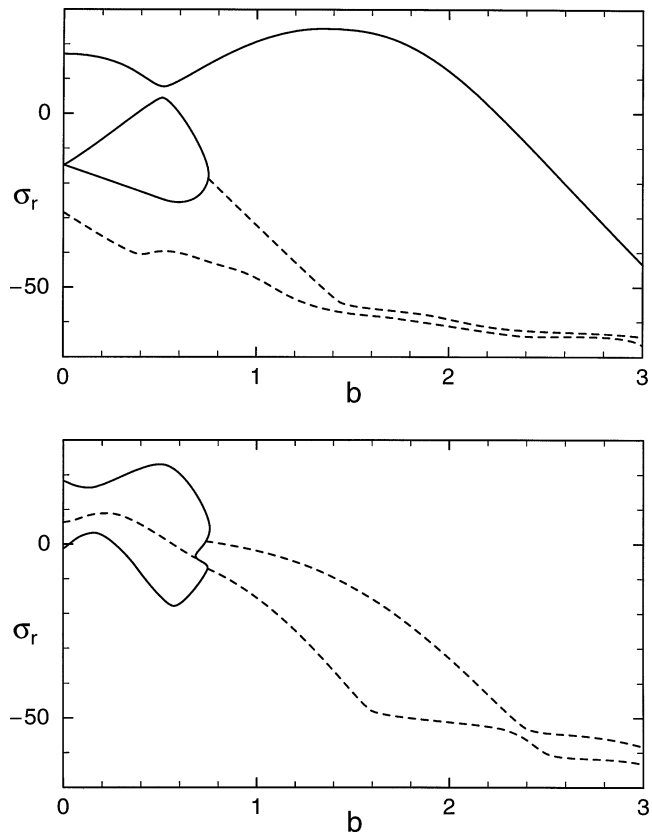

Figure 10. Growth rates σ_r for disturbances as a function of b in the case $\Omega = 17$, $Re = 600$, $a = 1.0$, $\varepsilon = 20°$. The upper (lower) graph corresponds to the upper (lower) solutions for the solitary vortex. Growth rates with vanishing (finite) imaginary parts are indicated by solid (dashed) lines.

Although it has not been possible to find a parameter regime where the solitary vortices described in this paper are stable, it is possible that they could be stabilized under inhomogeneous conditions. There thus still exists the possibility that they correspond to the solitary vortices or 'rollers' observed in experiments with rotating disks. A detailed numerical analysis will be required to establish such a correspondence.

References

[1] Schouveiler L., Le Gal P., Chauve M.P., Takeda Y., Experimental study of the stability of the flow between a rotating and a stationary disk, in: Gavrilakis S., Machiels L., Monkewitz P.A. (Eds), Advances in Turbulence VI, Proceedings of 6th European Turbulence Conference, Kluwer Acad. Publ., 1996, pp. 385–388.

[2] Hoffmann N., Busse F.H., Chen W.-L., Transitions to complex flows in the Ekman–Couette layer, J. Fluid Mech. 366 (1998) 311–331.

[3] San'kov P.I., Smirnov E.M., Bifurcation and transition to turbulence in the gap between rotating and stationary parallel disks, Fluid Dyn. 19 (1985) 695–702.

[4] Chandrasekhar S., Hydrodynamic and Hydromagnetic Stability, Clarendon Press, Oxford, 1961.

[5] Clever R.M., Busse F.H., Low Prandtl number convection in a layer heated from below, J. Fluid Mech. 102 (1981) 61–74.

[6] Cherhabili A., Ehrenstein U., Spatially localized two-dimensional finite-amplitude states in plane Couette flow, Eur. J. Mech. B/Fluids 14 (1995) 677–696.

[7] Cherhabili A., Ehrenstein U., Existence and stability of finite-amplitude states in plane Couette flow, in: Gavrilakis S., Machiels L., Monkewitz P.A. (Eds), Advances in Turbulence VI, Proceedings of 6th European Turbulence Conference, Kluwer Acad. Publ., 1996, pp. 317–320.